Resonant waves in elastic structured media: Dynamic homogenisation versus Green's functions

Alexander B. Movchan [a,*], Leonid I. Slepyan [b,c]

[a] Department of Mathematical Sciences, University of Liverpool, L69 7ZL, UK
[b] School of Mechanical Engineering, Faculty of Engineering, Tel Aviv University, P.O. Box 39040, Tel Aviv 6997801, Israel
[c] Department of Mathematics and Physics, Aberystwyth University, Physical Sciences Building, Aberystwyth, SY23 3BZ, UK

ARTICLE INFO

ABSTRACT

We address an important issue of dynamic homogenisation in vector elasticity for a doubly periodic mass-spring elastic lattice. The notion of logarithmically growing resonant waves is used in the analysis of star-shaped wave forms induced by an oscillating point force. We note that the dispersion surfaces for Floquet–Bloch waves in the elastic lattice may contain critical points of the saddle type. Based on the local quadratic approximations of a dispersion surface, where the radian frequency is considered as a function of wave vector components, we deduce properties of a transient asymptotic solution associated with the contribution of the point source to the wave form. The notion of local Green's functions is used to describe localised wave forms corresponding to the resonant frequency. The special feature of the problem is that, at the same resonant frequency, the Taylor quadratic approximations for different groups of the critical points on the dispersion surfaces (and hence different Floquet–Bloch vectors) are different. Thus, it is shown that for the vector case of micro-structured elastic medium there is no uniformly defined dynamic homogenisation procedure for a given resonant frequency. Instead, the continuous approximation of the wave field can be obtained through the asymptotic analysis of the lattice Green's functions, presented in this paper.

© 2014 Elsevier Ltd. All rights reserved.

1. Introduction

The subject of homogenisation is of great interest to physicists, engineers and mathematicians. The work in this area goes back more than 100 years, with the classical and elegant paper by Rayleigh (1892) being one of foundation stones in analysis of effective properties of periodic composite media. Mathematical theory of multi-scale homogenisation approximations has received a substantial attention, as comprehensively described in the books by Bensoussan et al. (1978), Sanchez-Palencia (1980), Marchenko and Khruslov (2006), Bakhvalov and Panasenko (1984) and Zhikov et al. (1994).

Conventional homogenisation in problems of wave propagation would normally apply to the case of long wave asymptotics, where a characteristic size of scatterers within a periodic structure is much smaller compared to the wavelength of the incident wave.

Resonant waves excited by a harmonic force in *uniform* square and triangular lattices were studied by Ayzenberg-Stepanenko and Slepyan (2008) in the framework of a scalar problem. It was shown that the resonant waves spread mainly on some separate rays to form star-like configurations and hence show strong dynamic anisotropy. This paper presented the underlining structure of such dynamics including the phenomenon of localisation. The scalar problem for the *nonuniform*, periodic square lattice was examined by Craster et al. (2009, 2010) where the localisation phenomena were also found for the scalar problem. The papers by Craster et al. (2009, 2010) also addressed the issue of a high-frequency homogenisation in the neighbourhood of the resonant modes for scalar formulations related to membrane-like lattice systems.

There has been a substantial advance in the definition and analysis of the effective constitutive equations in dynamic regimes. In this area, the pioneering approach was developed by Willis (1983), Willis (1984, 1997) and further advanced by Milton et al. (2006), Milton and Willis (2007), Nemat-Nasser and Srivastava (2011), Shuvalov et al. (2011), Willis (2011, 2012) and Norris et al. (2012).

Recent publications by Milton et al. (2006), Milton and Nicorovici (2006), Milton and Willis (2007), Norris (2008, 2012), Brun et al. (2009) on the dynamic response of metamaterials and

* Corresponding author. Tel: +44 151 7944740; fax: +44 51 7944056.
E-mail address: abm@liverpool.ac.uk (A.B. Movchan).

invisibility cloaks in elastic and acoustic media raised interesting questions related to approximating of such systems by multi-scale composites, that may possess such unusual properties as chirality, negative refraction and negative inertia. The range of frequencies in such applications would be well outside the standard homogenisation range, and hence the new approach is required.

The paper by Colquitt et al. (2012) addresses the vector problems for elastic Floquet–Bloch waves in a beam-made triangular lattice. The analysis of the dispersion relations has revealed a strong dynamic anisotropy with a certain range of frequencies. It has also shown the effects of negative refraction for a certain class of structured interfaces.

The concept of high-frequency homogenisation for problems of vector elasticity remains a challenge, as several critical points on a dispersion surface may exist for the same frequency, and these points may correspond to resonant modes of different physical nature. It is worth saying that the vector problem considered in this paper differs substantially from the scalar case. Namely, in the scalar problem, only one group of the related critical points on the dispersion surfaces corresponds to a given resonant frequency. This makes a unique homogenisation approximation possible in the case of a scalar dynamic lattice. On the contrary, in the case of the vector problem of elasticity, for the same resonant frequency there exist several different groups of critical points on the dispersion diagram, and this creates a subtlety in understanding of a dynamic homogenisation, as there is no uniqueness. This fact fundamentally changes the approach to the problem.

We address here these important issues for frequencies corresponding to resonant modes within a vector formulations for the mass-spring triangular elastic lattice. Also, we focus on analysis of lattice Green's tensors for a two-dimensional vector problem of elasticity and show how this powerful approach compares to multi-scale homogenisation approximations. This analysis incorporates asymptotic approximations for the resonant waves. The directional localisation is then associated with saddle points on the dispersion surfaces, which are also linked to the anisotropy in the dynamic regime. According to the structure of the dispersion relations, there exist several different wave forms corresponding to the same resonant frequency. Hence, different asymptotic solutions and homogenised equations may be derived for the same frequency. The subtlety is resolved by identifying the reference resonance modes and analysing the asymptotics of Green's tensors. We identify asymptotic solutions for logarithmically growing resonance waves, which, in the case of a saddle point, also resemble the star-shaped wave forms.

2. Governing equations for a forced elastic lattice

Consider a regular triangular lattice consisting of point masses connected by massless elastic links. The mass value, the bond length and stiffness are taken as the natural units. Thus, the lattice spacing along the bond line is equal to unity, whereas the distance between the parallel bond lines is $\sqrt{3}/2$. The lattice is subjected to a time-harmonic external force acting on a given mass. We would like to identify resonance modes, in particular those on the boundaries of the stop bands, and furthermore analyse homogenisation approximations corresponding to the resonant frequencies.

For the chosen geometry and physical parameters of the periodic lattice, in the long-wave/low-frequency approximation, we obtain a homogeneous, isotropic, elastic body, which is well-described in the existing literature. We refer to Slepyan, 2002, where the effective properties of this homogenised solids are outlined in detail. Namely, we have the effective normalised density $\varrho = 2/\sqrt{3}$, Poisson's ratio $\nu = 1/3$ and the following effective val-

ues for the speed of the longitudinal, shear and Rayleigh waves: $c_1 = \sqrt{9/8}$, $c_2 = \sqrt{3/8}$ and $c_R = \frac{1}{2}\sqrt{3 - \sqrt{3}}$, respectively. The effective shear modulus for such a lattice in the static approximation is $\mu = \sqrt{3}/4$.

It will be shown that in the time-harmonic regime, as the frequency increases, this lattice becomes far from being isotropic, and moreover, governing equations of the homogenised body may change its type from being elliptic to hyperbolic.

The displacement vector is denoted by $\boldsymbol{u}_{m,n} = (u_x, u_y)_{m,n} = (u, v)_{m,n}$, where the integers, m, n, define the mass position. In the Cartesian coordinates, x, y, we have

$$x = m + \frac{n}{2}, \quad y = \frac{\sqrt{3}}{2}n; \quad (m, n) = 0, \pm 1, \pm 2, \ldots. \tag{1}$$

The displacement components satisfy the equations of motion as follows

$$\ddot{u}_{m,n} = Q_0 - Q_3 + \frac{1}{2}(Q_1 - Q_2 - Q_4 + Q_5) + P_{x;m,n},$$

$$\ddot{v}_{m,n} = \frac{\sqrt{3}}{2}(Q_1 + Q_2 - Q_4 - Q_5) + P_{y;m,n}, \tag{2}$$

where $\boldsymbol{P}_{m,n} = (P_{x;m,n}, P_{y;m,n})$ are the external forces, applied to the (m, n) mass, whereas $Q_j, j = 0, 1, \ldots, 5$, are the forces acting on the mass (m, n) from the neighbouring masses, i.e.

$$Q_0 = u_{m+1,n} - u_{m,n}, \quad Q_3 = u_{m,n} - u_{m-1,n},$$

$$Q_1 = \frac{1}{2}(u_{m,n+1} - u_{m,n}) + \frac{\sqrt{3}}{2}(v_{m,n+1} - v_{m,n}),$$

$$Q_2 = -\frac{1}{2}(u_{m-1,n+1} - u_{m,n}) + \frac{\sqrt{3}}{2}(v_{m-1,n+1} - v_{m,n}),$$

$$Q_4 = -\frac{1}{2}(u_{m,n-1} - u_{m,n}) - \frac{\sqrt{3}}{2}(v_{m,n-1} - v_{m,n}),$$

$$Q_5 = \frac{1}{2}(u_{m+1,n-1} - u_{m,n}) - \frac{\sqrt{3}}{2}(v_{m+1,n-1} - v_{m,n}). \tag{3}$$

Assuming the time-harmonic vibrations with the amplitudes $\boldsymbol{U}_{m,n}$ and radian frequency ω, we have

$$\boldsymbol{u}_{m,n}(t) = \boldsymbol{U}_{m,n}e^{i\omega t}.$$

Correspondingly, the discrete Fourier transform gives

$$\boldsymbol{U}^{FF}(\boldsymbol{k}) = \sum_{m,n} \boldsymbol{U}_{m,n} \exp(i\boldsymbol{k} \cdot \boldsymbol{x}(m,n)), \tag{4}$$

where $\boldsymbol{x}(m, n)$ is the position vector of the (m, n)-mass. The same transform applies to the amplitude of the external force acting on the masses.

The original amplitudes are then defined by the inverse transform, which in our particular case, is given in the form

$$\boldsymbol{U}_{m,n} = \frac{\sqrt{3}}{16\pi^2} \int_{-2\pi/\sqrt{3}}^{2\pi/\sqrt{3}} \left(\int_{-2\pi}^{2\pi} \boldsymbol{U}^{FF}(\boldsymbol{k})e^{-i(\boldsymbol{k}\cdot\boldsymbol{x}(m,n))} \, dk_x \right) dk_y. \tag{5}$$

3. Elastic compliance and dispersion

We assume that the external load is represented by a time-harmonic point force with the amplitude vector $\boldsymbol{P}_{0,0} = \boldsymbol{P} = (P_x, P_y), |\boldsymbol{P}| = 1$, acting on the central mass, $m = n = 0$. With this in mind we find from (2) that

$$\boldsymbol{U}^{FF} = \boldsymbol{A}_{\omega,\boldsymbol{k}}\boldsymbol{P}, \tag{6}$$

where $\boldsymbol{A}_{\omega,\boldsymbol{k}}$ is the compliance symmetric tensor, given by

$$\boldsymbol{A}_{\omega,\boldsymbol{k}} = \boldsymbol{B}_{\omega,\boldsymbol{k}}/\Delta. \tag{7}$$

Here

$$B_{xx} = -\Omega + 3\left(1 - \cos\left(\frac{k_x}{2}\right)\cos\left(\frac{\sqrt{3}}{2}k_y\right)\right),$$

$$B_{xy} = B_{yx} = -\sqrt{3}\sin\left(\frac{k_x}{2}\right)\sin\left(\frac{\sqrt{3}}{2}k_y\right),$$

$$B_{yy} = -\Omega + 2(1 - \cos k_x) + 1 - \cos\left(\frac{k_x}{2}\right)\cos\left(\frac{\sqrt{3}}{2}k_y\right), \quad \Omega = \omega^2 \quad (8)$$

and the function $\Delta(\omega, k_x, k_y)$ can be factorised in the form

$$\Delta = (\Omega - \Omega_1)(\Omega - \Omega_2), \quad \Omega_{1,2} = \omega_{1,2}^2 = F \pm \sqrt{S}. \tag{9}$$

The quantities F and S are periodic functions of k_x and k_y defined as follows

$$F = 1 - \cos k_x + 2\left(1 - \cos\left(\frac{k_x}{2}\right)\cos\left(\frac{\sqrt{3}}{2}k_y\right)\right),$$

$$S = \left(\cos k_x - \cos\left(\frac{k_x}{2}\right)\cos\left(\frac{\sqrt{3}}{2}k_y\right)\right)^2 + 3\sin^2\left(\frac{k_x}{2}\right)\sin^2\left(\frac{\sqrt{3}}{2}k_y\right). \tag{10}$$

The dispersion of waves in the elastic lattice is governed by the equation

$$\Delta(\omega, k_x, k_y) = 0. \tag{11}$$

Two dispersion surfaces, periodic in k_x and k_y, are identified by the equations

$$\Omega - \Omega_{1,2} = 0.$$

On the elementary cell of periodicity, these surfaces have common points, where $\Omega_1 = \Omega_2 = 0$, at the origin, $k_x = k_y = 0$, and at the corner points $k_x = \pm 2\pi$, $k_y = \pm 2\pi/\sqrt{3}$, where there is also $\Omega_{1,2} = 0$. Additional detailed explanation is below. The graphs of the dispersion surfaces $\omega = \omega_{1,2}(k_x, k_y)$ restricted to the elementary cell of periodicity are presented in Figs. 1 and 2.

4. Resonant excitation. Asymptotics of Green's kernels

Floquet–Bloch waves and their dispersion properties are important for evaluation of resonant frequencies within a periodic system. We refer to Ayzenberg-Stepanenko and Slepyan (2008), and Colquitt et al. (2012) who have analysed the resonant forms and
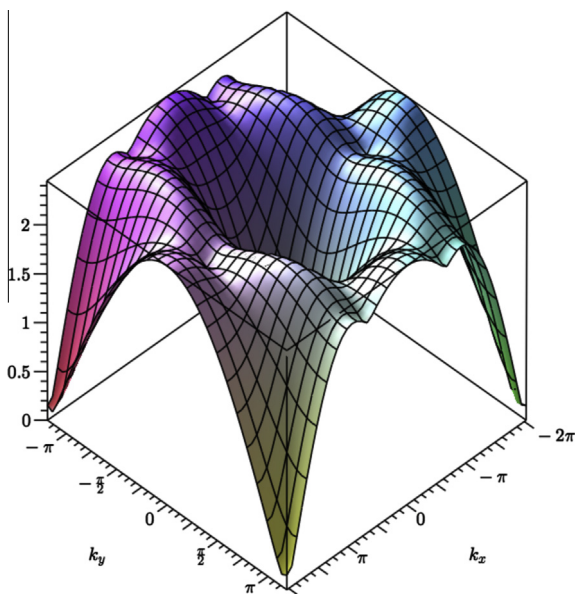

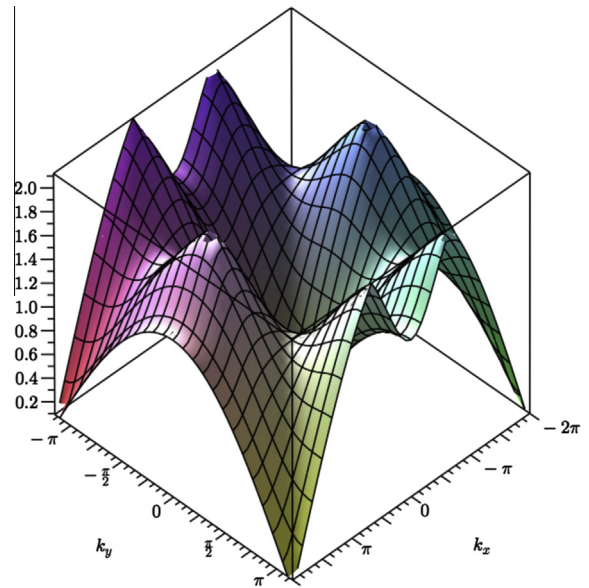**Fig. 1.** Dispersion surfaces $\omega = \omega_1(k_x, k_y)$.

Fig. 2. Dispersion surface $\omega = \omega_2(k_x, k_y)$.

star-shaped waves in lattices as well as features of dynamic anisotropy for elastic waves in an elastic triangular lattice.

Note that there is a fundamental difference between the "near resonance" and the exact case of resonance frequencies. For uniformly distributed systems, a steady mode of forced waves/oscillations exists in a non-resonant case, whereas, in general, no such a mode exists for forced waves/oscillations at the resonant frequency. Indeed, there exist so-called standing waves. However, these are considered as free waves/oscillations but not as the forced ones. Here it will be shown that by considering the resonant case we have to deal with a transient problem.

4.1. Critical points on the dispersion surfaces

A critical point (k_x^*, k_y^*, ω^*) on a smooth dispersion surface $\omega = \omega(k_x, k_y)$ is defined in the classical sense: $\partial\omega/\partial k_x(k_x^*, k_y^*) = \partial\omega/\partial k_y(k_x^*, k_y^*) = 0$. In other words, a tangent plane at a critical point is parallel to the (k_x, k_y) plane, and consequently the group velocity of the corresponding Floquet–Bloch wave equals zero; a wave with the zero group velocity is referred to as a *standing wave*. The corresponding forced wave at (k_x^*, k_y^*, ω^*) is the resonant one, and hence we also refer to (k_x^*, k_y^*, ω^*) as the resonant point. Three resonant values of the frequency are considered below. The resonant points at the highest frequency are of the parabolic type (these are the points of maximum), whereas the other critical points appear to be the saddle points. The latter cases are of great interest, as they correspond to transient, directionally-localised, growing forced waves.

The critical points on the dispersion surfaces, corresponding to standing waves, are identified by the resonant frequencies, ω_i^*, and components of the Bloch vector, as shown in Table 1 below.

We note that there are multiple critical points identified for the same frequency, which makes classical homogenisation impossible. However, we intend to analyse the profile of the dispersion surface in the neighbourhoods of individual critical points and hence identify standing waves and furthermore resonant excitation modes.

The dispersion surfaces crossed by fixed-frequency planes are presented in Figs. 3–5: in the first of these diagrams, the plane is taken slightly below the points of maximum, $\omega = \omega_1^* - 0.02$, to make the location of the points visible; in the diagrams (b) and

Table 1
Positions of critical points on the dispersion surfaces, as defined by components of the Bloch vector (k_x, k_y) and the radian frequency ω^*.

i, ω_i^*	$(k_{x;i1}, k_{y;i1})$	$(k_{x;i2}, k_{y;i2})$	$(k_{x;i3}, k_{y;i3})$
$1, \sqrt{6}$	$(0, \pm 2\pi/\sqrt{3})$	$(\pm 2\pi, 0)$	$(\pm \pi, \pm 1.8137994)$
$2, 2.25$	$(\pm 2.8909370, \pm 2\pi/\sqrt{3})$	$(\pm 3.3922483, 0)$	$(\pm 1.6961242, \pm 2.9377732)$
			$(\pm 4.5870611, \pm 0.6898255)$
$3, \sqrt{2}$	$(0, \pm 2\pi/\sqrt{3})$	$(\pm 2\pi, 0)$	$(\pm \pi, \pm \pi/\sqrt{3})$

(c) the critical points are the saddle points on the dispersion surfaces.

The resonant-frequency dispersion contours are plotted in Figs. 6–8. As shown in Table 1 (also illustrated by slowness contours), there exist 8, 14 and 8 resonant points at the resonant frequencies ω_1^*, ω_2^* and ω_3^*, respectively. In particular, the critical points corresponding to the frequencies ω_2^* and ω_3^* are the saddle points on the dispersion surfaces, whereas $\omega = \omega_1^*$ represents the points of maximum on the dispersion surface (see Fig. 6). Note the connection between Figs. 7, 8 and 4, 5 respectively. Whereas the formulae (7) and (10) define analytically the dispersion surfaces in Fig. 4 and 5 the Figs. 7 and 8 show the cross-points of the slowness contours, which correspond to the saddle points of the surfaces $\omega = \omega_{1,2}(k_x, k_y)$.

4.2. Resonant versus non-resonant excitations

First, we evaluate $\boldsymbol{B}_{\omega,\boldsymbol{k}}$, as in (8), at the resonant points. The required values are presented in Table 2 below.

As follows from (9), the two dispersion surfaces, $\omega = \omega_{1,2}(k_x, k_y)$, intersect at the points, where $S = 0$, and only at these points. The function S is defined by (10), as a sum of two non-negative terms; $S = 0$ implies $k_x = 0, \pm 2\pi, k_y = 0, \pm 2\pi/\sqrt{3}$. At these points $F = 0$, and according to (9), $\omega = 0$ at the points of intersection. Thus the dispersion surfaces $\omega = \omega_{1,2}(k_x, k_y)$ can intersect only at zero frequency. We also note that no growing wave is excited by an action corresponding to zero values of B_{xx}, B_{yy} or $B_{x,y}$ presented in Table 2.

The representation (6) is valid for non-resonant excitations, where $\Delta \neq 0$. There is no such a steady state in the resonant case, and a transient problem should be considered. For the transient problem we have to replace Ω by $-\partial^2/\partial t^2$. In this way, for the fol-
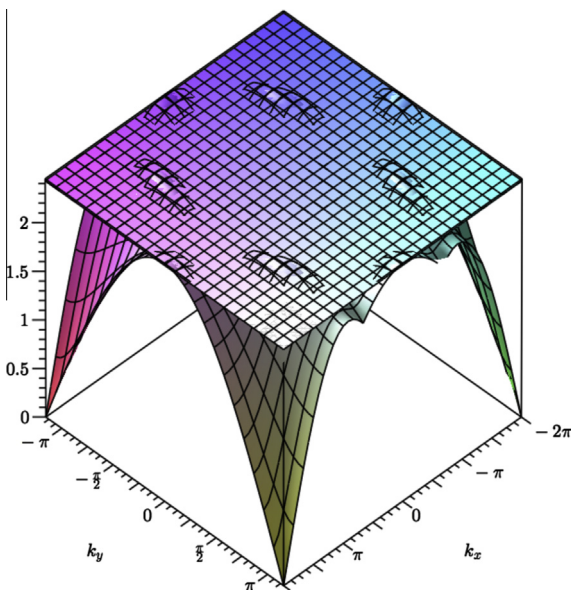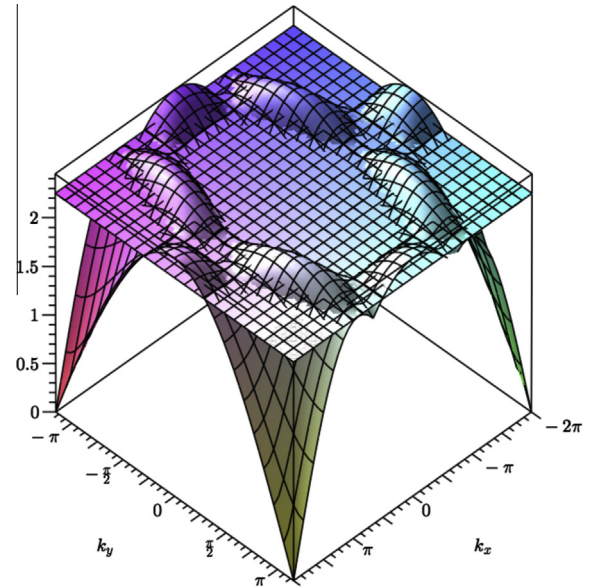

Fig. 4. Dispersion surface $\omega = \omega_1(k_x, k_y)$ intersecting with the plane $\omega = \omega_2^*$.
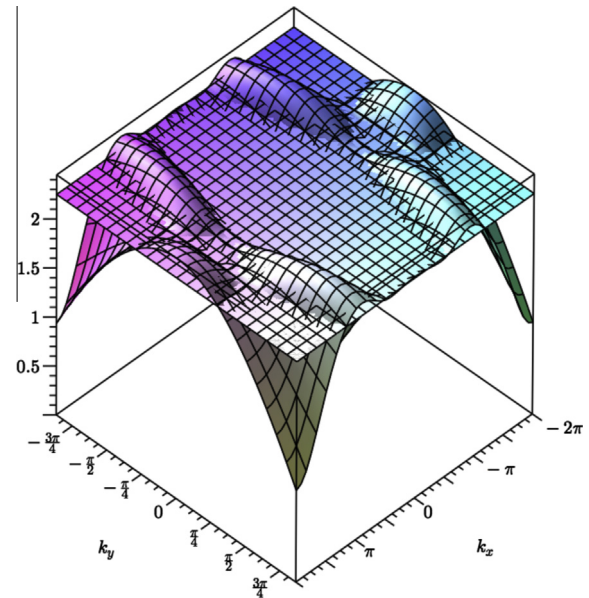

Fig. 5. Dispersion surface $\omega = \omega_2(k_x, k_y)$ intersecting with the plane $\omega = \omega_3^*$.

lowing considerations the Laplace transform on t is useful, and a formulation for the resonant harmonic excitation is obtained substituting $\Omega = -s^2$ and $\boldsymbol{P}e^{i\omega t} \to \boldsymbol{P}/(s - i\omega)$, where s is the Laplace transform parameter. Thus, we have

$$\boldsymbol{u}^{FFL} = \frac{\boldsymbol{BP}}{(s - i\omega)\Delta}. \tag{12}$$

4.3. The dispersion relations in vicinities of the resonant points and the characteristic lines

The quadratic terms of the power expansion of $\Omega(\Omega_1 \text{ or } \Omega_2)$

$$\Omega - (\omega_i^*)^2 \sim a_{ij}q_x^2 + b_{ij}q_y^2 + c_{ij}q_xq_y(k_{x,y} - k_{x,y:ij} = q_{x,y:ij} \to 0) \tag{13}$$

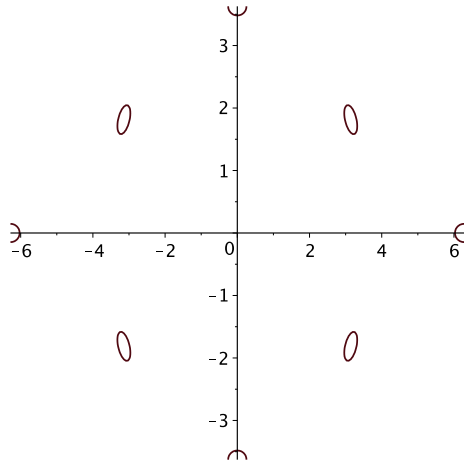**Fig. 3.** Dispersion surface $\omega = \omega_1(k_x, k_y)$ intersecting with the plane $\omega = \omega_1^* - 0.02$.

Fig. 6. The trace of the ω_1-surface crossed by the plane $\omega = \omega_1^* - 0.02$. Note that a small negative shift from the resonant frequency has been used to show the slowness contours in the vicinity of critical points.

Table 2
Coefficients B_{xx}, B_{yy}, B_{xy} in the representation (8) of the elastic compliance.

ij	B_{xx}	B_{yy}	B_{xy}
11/12	0	−4	0
13	−3	−1	$-\sqrt{3}$
21/22	−1.6875	0	0
23/24	−0.421875	−1.265625	−0.730709
31/32	4	0	0
33	1	3	$-\sqrt{3}$

for neighbourhoods of the resonant points located in the first quadrant, $0 \leqslant k_{x:ij} \leqslant 2\pi$, $0 \leqslant k_{y:ij} \leqslant 2\pi/\sqrt{3}$, are presented in Table 3:

The polynomial in (13) corresponds to the differential operator

$$E = a_{ij}\frac{\partial^2}{\partial x^2} + b_{ij}\frac{\partial^2}{\partial y^2} + c_{ij}\frac{\partial^2}{\partial x \partial y}. \tag{14}$$

The resonant points on the dispersion surfaces at $\omega = \omega_{2,3}^*$ are the saddle points, where the coefficients a_{ij} and b_{ij} are nonzero and different by the sign. Thus, the equation $E = 0$ is hyperbolic at these frequencies. It is satisfied by an arbitrary function of $\phi x - y$ with

$$\phi = \frac{c}{2a} \pm \sqrt{\left(\frac{c}{2a}\right)^2 - \frac{b}{a}}, \quad (a,b) = (a_{ij}, b_{ij}). \tag{15}$$

In addition, if $c_{ij} \neq 0$, due to the symmetry there exist another saddle point with $c_{ij1} = -c_{ij}$. This results in additional values of the parameter ϕ with a different sign of the first term in (15). Therefore the slopes of the characteristic lines are given by the angles relative to the x-axis

$$\alpha = \pm \arctan\left(\frac{c}{2a} \pm \sqrt{\left(\frac{c}{2a}\right)^2 - \frac{b}{a}}\right). \tag{16}$$

Table 3
Coefficients of the quadratic approximation (13) in the vicinity of critical points of dispersion surfaces.

ij	a_{ij}	b_{ij}	c_{ij}
11/12	−0.375	−1.125	0
13	−0.9375	−0.5625	−0.649519
21/22	−0.984375	1.265625	0
23/24	0.703125	−0.421875	−1.94856
31,32	0.875	−0.375	0
33	−0.0625	0.5625	−1.082532

The values of such angles for the rays associated with the saddle points of the dispersion surfaces are summarised in Table 4.

It follows that the critical rays for $\omega = \omega_2^*$ and $\omega = \omega_3^*$ are oriented symmetrically with respect to each lattice bond line as should be, namely

$$\alpha = \pm 0.19913547 + \frac{\pi n}{3}(\omega = \omega_2^*), \quad \alpha = \pm 0.46755781$$
$$+ \frac{\pi n}{3}(\omega = \omega_3^*), \quad n = 0, 1, \dots, 5, \tag{17}$$

where the directional angle $\alpha = 0$ corresponds to a bond line.

4.4. Green's tensor asymptotics

Substituting $s = i\omega + s'$ in (12) we obtain the following expressions for the oscillation amplitudes

$$\boldsymbol{U}^{FFL} = (\boldsymbol{u}e^{-i\omega t})^{FFL} = \frac{\boldsymbol{BP}}{s'\Delta} \tag{18}$$

with

$$\Delta = [(s' + i\omega)^2 + \Omega_1][(s' + i\omega)^2 + \Omega_2]. \tag{19}$$

To proceed we now note that for a resonant frequency, $\omega = \omega_i^*$, the amplitude growing in time is defined by integration in (5) in the vicinities of the resonant points where Ω_1 or Ω_2 is equal to $(\omega_i^*)^2$. We note that $\Omega - (\omega_i^*)^2 \to 0$ as $\boldsymbol{k}$ tends to a resonant point. It follows from this that for the asymptotic representation of the resonant oscillation amplitude we need to consider the case as $s' \to 0$. In this way, putting $(s' + i\omega)^2 \sim -\omega^2 + 2i\omega s'$ we obtain the following asymptotic relation of Δ associated with a resonant point

$$\Delta \sim C\left[s' - i\left(aq_x^2 + bq_y^2 + cq_xq_y\right)\right], \tag{20}$$

where the constant C is different for different resonant frequencies, i.e.

$$C = 2i\omega(\Omega_1 - \omega^2)(\omega = \omega_3^*), \quad C = 2i\omega(\Omega_2 - \omega^2)(\omega = \omega_{1,2}^*). \tag{21}$$

In turn, the coefficients a, b, c are summarised in Table 3.

Using the relation in (20) for the asymptotic regime, $t \to \infty$, $\boldsymbol{x}/t \to 0$, the integration in the Fourier inverse transform can be extended over the whole $\boldsymbol{k}$ plane. It follows that the wave associated with a saddle point (ij), associated with the resonance frequency ω_i^*, is asymptotically defined as

$$\boldsymbol{u}_{ij} \sim \boldsymbol{U}_{ij}\exp[i(\omega_i^* t - \boldsymbol{k}_{ij} \cdot \boldsymbol{x})], \quad \text{and} \quad \partial\boldsymbol{U}_{ij}/\partial t$$
$$= \dot{\boldsymbol{U}}_{ij} \sim \frac{\sqrt{3}}{16\pi^2 C}V.p.\int_{-\infty}^{\infty}\int_{-\infty}^{\infty}\exp[i(t(aq_x^2 + bq_y^2 + cq_xq_y)$$
$$- xq_x - yq_y)]\,dq_x\,dq_y\boldsymbol{B}_{ij}\boldsymbol{P} = \frac{\sqrt{3}}{8\pi C\sqrt{c^2 - 4ab}\,t}\exp(iR)\boldsymbol{B}_{ij}\boldsymbol{P},$$
$$R = \frac{bx^2 + ay^2 - cxy}{(c^2 - 4ab)t}, \quad (a,b,c) = (a,b,c)_{ij}. \tag{22}$$

It follows that the asymptotic approximation for the displacement amplitude is given by

$$\boldsymbol{U}_{ij} = \int_0^t \dot{\boldsymbol{U}}_{ij}dt \sim \frac{\sqrt{3}}{8\pi C\sqrt{c^2 - 4ab}}\text{Ei}(1, -iR)\boldsymbol{B}_{ij}\boldsymbol{P} \tag{23}$$

Table 4
Coefficients of the quadratic approximation (13) in the vicinity of critical points of dispersion surfaces.

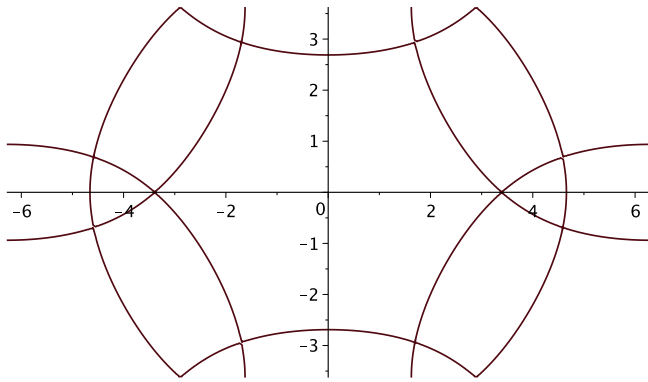| ij	α
21, 22	$\pm(\pi/3 - \lambda_2), \pm(2\pi/3 + \lambda_2)(\lambda_2 = 0.19913547)$
23/24	$\pm\lambda_2, \pi \pm \lambda_2, \pm(\pi/3 + \lambda_2), \pm(2\pi/3 - \lambda_2)$
31,32	$\pm(\pi/3 - \lambda_3), \pm(2\pi/3 + \lambda_3)(\lambda_3 = 0.46755781)$
33	$\pm\lambda_3, \pi \pm \lambda_3, \pm(\pi/3 + \lambda_3), \pm(2\pi/3 - \lambda_3)$

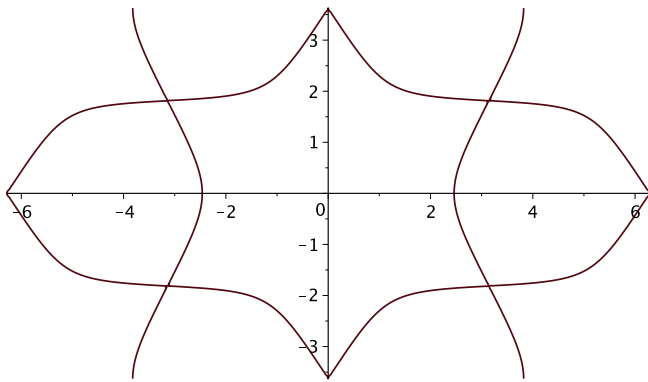**Fig. 7.** Resonant-frequency slowness diagram, $\omega_1 = \omega_2^* = 2.25$.

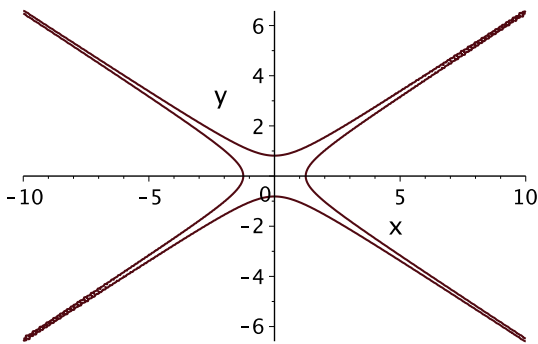**Fig. 8.** Resonant-frequency slowness diagram, $\omega_2 = \omega_3^* = \sqrt{2}$.

Fig. 9. The star-wave configuration associated with the resonant point 31, $t = 2000$, $|Ei(1, -iR)| = 8$.
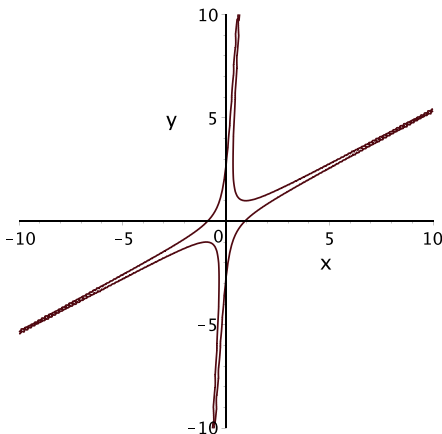

Fig. 10. The star-wave configuration associated with the resonant points 33 in the first and third quadrants of the k_x, k_y-plane, $t = 2000$, Ei $(1, -iR) = 8$.
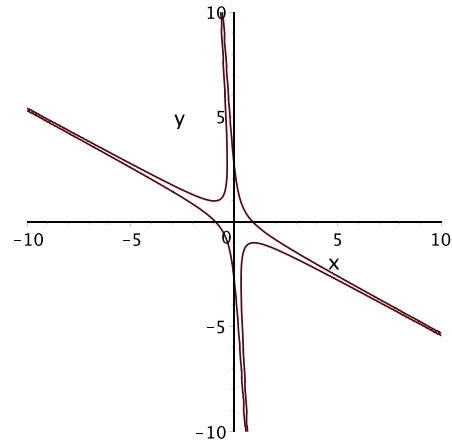

Fig. 11. The star-wave configuration associated with the resonant point $\omega = \omega_3^*$ in the second and fourth quadrants of the k_x, k_y-plane, $t = 2000$, Ei $(1, -iR) = 8$.

and

$$
Ei(1, iR) = -Ci(|R|) + i\left[Si(R) - \frac{\pi}{2} \text{sign}R\right]
$$
$$
\sim -\ln|R| - \gamma - i\frac{\pi}{2}\text{sign}R(|R| \ll 1), \tag{24}
$$

where γ is Euler's constant.

The above asymptotic solution is valid outside the characteristic line, $R = 0$, where it becomes singular. To evaluate the wave amplitude on this line, one needs higher-order terms in the Taylor expansion of the dispersion surface near a critical point. Note that the characteristic lines defined by the equation $R = 0$ coincide with those in (16).

A typical star-shaped wave form associated with a saddle point is shown in Fig. 9, where the level lines are plotted. Note that for this symmetric wave the coefficient c_{ij} in (14) is equal to zero. In Figs. 10, 11, we show the wave forms represented by the level lines of the amplitude of the displacement along the horizontal bond, u_x, for Ei$(1, R) = 3$ at $t = 400$. The amplitude is greater inside the star and lower outside it. The resonant waves excited at $\omega = \omega_3^*$ are shown in Figs. 12 and 13.

5. Homogenisation and concluding remarks

In accordance with (14) and (20), the homogenised equation for $\dot{U}$ associated with a resonant point is

$$
a\frac{\partial^2 \dot{U}}{\partial x^2} + b\frac{\partial^2 \dot{U}}{\partial y^2} + c\frac{\partial^2 \dot{U}}{\partial x \partial y} - i\frac{\partial \dot{U}}{\partial t} = \frac{BP}{C}, \tag{25}
$$

where the coefficients, a, b, c, are generally different for different resonant points (see (20), (21) and Table 3). For a saddle resonant point, $ab < 0$, this equation is hyperbolic and the critical rays on the (x, y)-plane correspond to its characteristics. The solution to this equation is presented in (22), (23).

Recall that different homogenisation corresponds to different resonant points at the same frequency. This does not allow for a global homogenisation, which could correspond to a given resonant frequency. Instead, the global asymptotic Green's tensor is built, which represents the continuous approximation of the wave field. In conclusion, note that while the Green's tensor is defined by the inverse transforms, the directions of the resonant wave localisation can be seen in the resonant-frequency dispersion contours. Indeed, (a) the excited propagation waves correspond to the level lines since the other free waves have different frequencies; (b) the contribution to the resonant wave is not given by the resonant point itself but by a set of the waves corresponding to the level
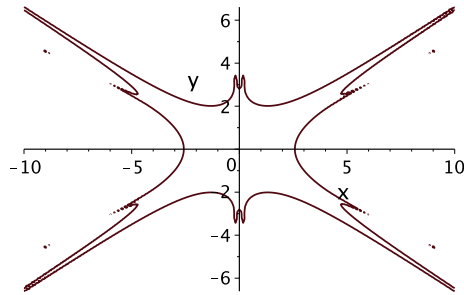
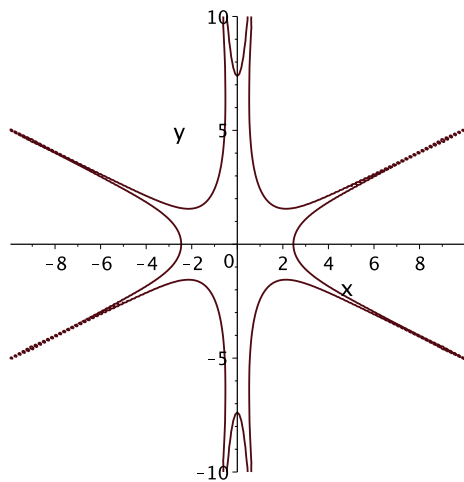**Fig. 12.** The resonant wave excited by the horizontal unit force, $P_x = 1, P_y = 0$ at $\omega = \omega_3^*, t = 2000, |\boldsymbol{U}| = 0.2$.

Fig. 13. The resonant wave excited by the vertical unit force, $P_x = 0, P_y = 1$ at $\omega = \omega_3^*, t = 2000, |\boldsymbol{U}| = 0.2$.

lines in a vicinity of the former; (c) the group velocities of the latter are directed along the normal to the level line. Thus, the 'star' directions coincide with the normals to the level lines at the saddle resonant points, that is, at the cross- and angle points of the lines. Note that the energy transfer in 1D resonant waves is considered in Slepyan and Tsareva (1987).

Acknowledgment

References

Ayzenberg-Stepanenko, M., Slepyan, L.I., 2008. Resonant-frequency primitive waveforms and star waves in lattices. J. Sound Vib. 313, 812–821. http://dx.doi.org/10.1016/j.jsv.2007.11.047.

Bakhvalov, N.S., Panasenko, G.P., 1984. Homogenization: averaging processes in periodic media. Mathematics and Its Applications (Soviet Series), vol. 36. Kluwer Academic Publishers, Dordrecht-Boston-London.

Bensoussan, A., Lions, J.L., Papanicolaou, G., 1978. Asymptotic Analysis for Periodic Structures. North-Holland, Amsterdam.

Brun, M., Guenneau, S.R.L., Movchan, A.B., 2009. Achieving control of in-plane elastic waves. Appl. Phys. Lett. 94, 061903.

Colquitt, D.J., Jones, I.S., Movchan, N.V., Movchan, A.B., McPhedran, R.C., 2012. Dynamic anisotropy and localization in elastic lattice systems. Waves Random Complex Media 22 (2), 143–159.

Craster, R.V., Nolde, E., Rogerson, G.A., 2009. Mechanism for slow waves near cutoff frequencies in periodic waveguides. Phys. Rev. B 79, 045129.

Craster, R.V., Kaplunov, J., Postnova, J., 2010. High-frequency asymptotics, homogenisation and localisation for lattices. Q. J. Mech. Appl. Math. 63 (4), 497–519.

Marchenko, V.A., Khruslov, E.Y., 2006. Homogenization of Partial Differential Equations. Springer, Heidelberg.

Milton, G.W., Nicorovici, N.A., 2006. On the cloaking effects associated with anomalous localized resonance. In: Proc. Royal Soc. Ser. A, vol. 462. No 2074, pp. 3027–3059.

Milton, G.W., Willis, J.R., 2007. On modifications of Newtons second law and linear continuum elastodynamics. Proc. R. Soc. A 463, 855–880.

Milton, G.W., Briane, M., Willis, J.R., 2006. On cloaking for elasticity and physical equations with a transformation invariant form. New J. Phys. 8, 248. http://dx.doi.org/10.1088/1367-2630/8/10/248.

Nemat-Nasser, S., Srivastava, A., 2011. Overall dynamic constitutive relations of layered elastic composites. J. Mech. Phys. Solids 59, 1953–1956.

Norris, A.N., 2008. Acoustic cloaking theory. In: Proc. Royal Soc. Ser. A, vol. 464. No 2097, pp. 2411–2434.

Norris, A.N., Shuvalov, A.L., Kutsenko, A.A., 2012. Analytical formulation of three-dimensional dynamic homogenization for periodic elastic systems. In: Proc. R. Soc. A, published online, http://dx.doi.org/10.1098/rspa.2011.0698.

Rayleigh, Lord, 1892. On the influence of obstacles arranged in rectangular order upon the properties of a medium. Philos. Mag. 34, 481–502.

Sanchez-Palencia, E., 1980. Non-Homogeneous Media and Vibration Theory, Springer Lecture Notes in Physics, vol. 127. Heidelberg.

Shuvalov, A.L., Kutsenko, A.A., Norris, A.N., Poncelet, O., 2011. Effective Willis constitutive equations for periodically stratified anisotropic elastic media. Proc. R. Soc. A 467, 1749–1769.

Slepyan, L.I., 2002. Models and Phenomena in Fracture Mechanics. Springer-Verlag, Berlin, New York.

Slepyan, L.I., Tsareva, O.V., 1987. Energy flux for zero group velocity of the carrying wave. Sov. Phys. Dokl. 32, 522–524.

Willis, J.R., 1983. The overall elastic response of composite materials. J. Appl. Mech. ASME 50, 1202–1209.

Willis, J.R., 1984. Variational principles for dynamic problems for inhomogeneous elastic media. Wave Motion 3, 1–11.

Willis, J.R., 1997. Dynamics of composites. Continuum Micromechanics: CISM Lecture Notes, ch. 1, vol. 495. Springer, Vienna, Austria, pp. 265–290.

Willis, J.R., 2011. Effective constitutive relations for waves in composites and metamaterials. Proc. R. Soc. A 467, 1865–1879.

Willis, J.R., 2012. The construction of effective relations for waves in a composite. Comptes Rendus Mécanique 340, 181–192.

Zhikov, V.V., Kozlov, S.M., Oleinik, O.A., 1994. Homogenization of differential operators and integral functionals. Springer, Heidelberg.